Statistical analysis of bubble parameters from a model bubble column with and without counter-current flow

P. Kováts[1,*], K. Zähringer[1]
1: Laboratory of Fluid Dynamics and Technical Flows, Otto-von-Guericke-Universität Magdeburg. Universitätsplatz 2, D-39106 Magdeburg, Germany
* Correspondent author: peter.kovats@ovgu.de

Keywords: bubble aspect ratio, bubble size, bubble column, counter-current, CO_2

ABSTRACT

Bubble columns are widely used in numerous industrial processes, because of their advantages in operation, design and maintenance compared to other multiphase reactor types. In contrast to their simple design, the generated flow conditions inside a bubble column reactor are quite complex, especially in continuous mode with counter-current liquid flow. For the design and optimization of such reactors precise numerical simulations and modelling is needed. These simulations and models have to be validated with experimental data. For this reason experiments were carried out in a laboratory-scale bubble column with shadow imaging technique with and without counter-current liquid flow. In the experiments two types of gases –relatively badly soluble air and good soluble CO_2 – are applied and the bubbles were generated with three different capillary diameters. With changing gas and liquid flow rates overall 108 different flow conditions were investigated. The gathered data has been statistically evaluated over the whole 1 m measurement area and bubble parameters have been obtained such as bubble diameter, velocity, aspect ratio, bubble motion direction and inclination. The analysis of these parameters shows, that the counter-current liquid flow has a noticeable influence on the bubble parameters, especially on the bubble velocity and motion direction. In the case of CO_2 bubbles remarkable bubble shrinkage has been observed at counter-current liquid flow due to the enhanced mass transfer. The comprehensive and extensive bubble data obtained in this study will now be used as a source for the validation of numerical simulations and models.

1. Introduction

Bubble column reactors are simple multiphase contactors, where the gas phase is dispersed in the continuous phase. Since they have no moving parts, the operation and maintenance of these reactors is simple. Bubble columns in batch mode are widely used in chemical, biochemical and petrochemical industries. However e.g. in water and wastewater treatment, counter-current flow of liquid and gas is applied to increase the gas holdup and enhance mixing and mass transfer. The optimization of these two-phase reactors and processes often relays on numerical simulations and models. For the validation of such calculations detailed experimental data is needed. In this study we present the statistical evaluation of bubble parameter data (e.g. shape,

motion, size) from bubbles rising in a swarm in a laboratory-scale bubble column obtained by shadow imaging for a wide range of bubble sizes with and without counter-current flow. Shadow imaging combined with PTV (Particle Tracking Velocimetry) has been used to initially determine bubble size, shape and velocity. From this original data further parameters have been derived as e.g. bubble aspect ratio, bubble motion direction, bubble inclination. Thanks to the high number of initially acquired images and thus individual bubbles, a statistical evaluation of all these quantities was possible, not only for the complete column, but also depending on the heights in the column. This kind of data can now serve further for the evaluation of models or as validation data for numerical codes as e.g. needed in (Rzehak et al., 2017; Sommerfeld et al., 2018; Mühlbauer et al., 2019).

2. Initial experiments

The shadow imaging measurements have been executed in a quadratic laboratory-scale bubble column made of acryl glass with an inner side length of d=0.100 m and a height of h=2 m (Fig. 1, 1). A bubble curtain was generated with 7 capillaries placed in line in the centre of the bubble column (Fig. 1, 3) and bubbles in a size range of 1 to 9 mm are produced by introducing CO_2 or air through different diameter capillaries (0.13 mm, 0.18 mm and 3.6 mm). Gas flow rates from 1.3 $l \cdot h^{-1}$ up to 48 $l \cdot h^{-1}$ (2.4 to 57.5 $g \cdot h^{-1}$ mass flow rate; $3.6 \cdot 10^{-6}$ to $1.3 \cdot 10^{-4}$ $m \cdot s^{-1}$ superficial gas velocity) were investigated in stagnant liquid and at five different counter-current liquid flow conditions. The images have been recorded with four 5 Mpixel sCMOS cameras (LaVision Imager sCMOS) (Fig. 1, 2) equipped with 50 mm Nikon Micro lenses to simultaneously record all bubbles over the entire measurement section (1 m) of the column (Fig. 1, 4). The cameras were focused to the centre of the column. Therefore the bubbles in a 33 mm (±16.6 mm from the centre) thick volume in the centre of the column were evaluated, while the bubbles beyond this depth of field were unfocused and not taken into account. Eight high-power LEDs were used together with a sheet of thin drawing paper, as light diffusor, on the back wall of the column to obtain homogeneous light distribution. The geometrical calibration was performed in the whole measurement area with a half meter long 3D calibration plate. With this experimental setup 4000 pictures were taken with 80 Hz recording rate for each investigated case.

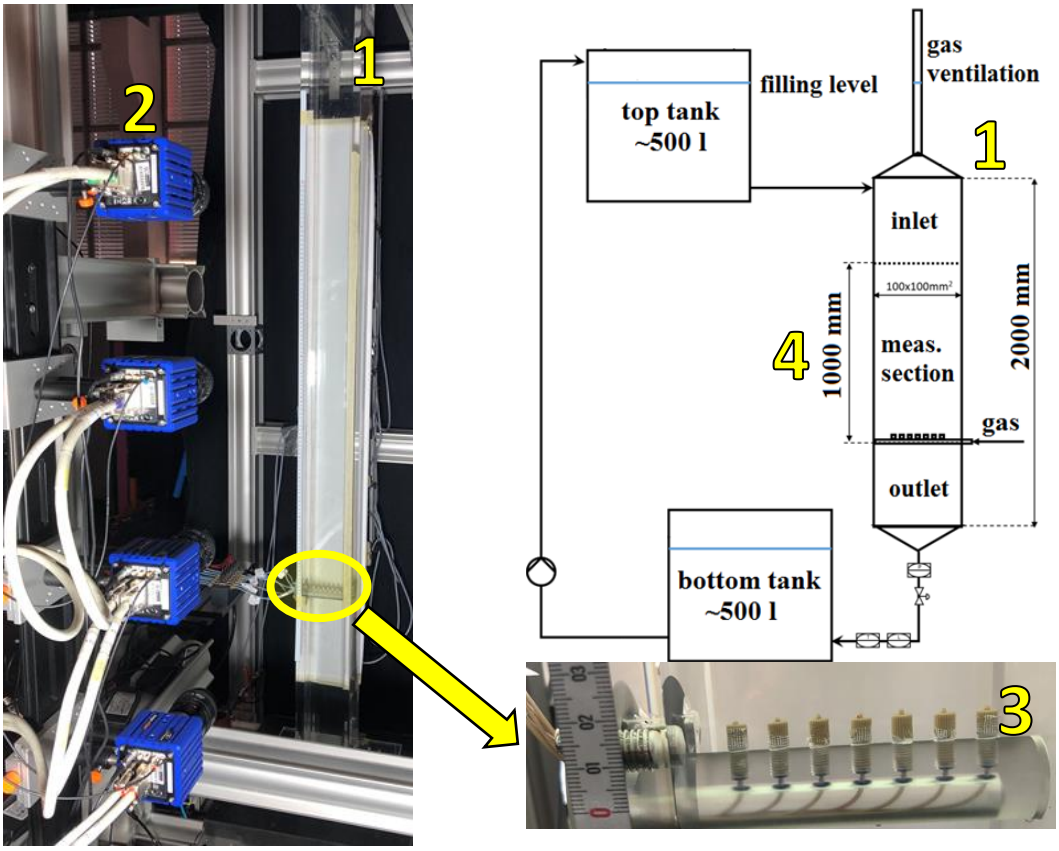

Fig. 1 Experimental setup for shadow imaging.

The experiments were carried out at three different gas flow rates for air and CO_2. Considering also the three capillary diameters and the six liquid flow conditions, it results in 108 different investigated cases (**Table 1**).

Table 1 Investigated cases.

Capillary id./ material	Gas	Superficial gas velocity [m · s^{-1}]	Gas flow rate [l · h^{-1}]	Gas mass flow rate [g · h^{-1}]	Superficial liquid velocity [m · s^{-1}]	Counter-current liquid flow [l · min^{-1}]	Reynolds number $\left(Re = \frac{d \cdot v_{Ls} \cdot \rho_L}{\mu_L}\right)$
0.13 mm/ stainless steel	Air	5.6 · 10^{-6} 1.7 · 10^{-5} 2.8 · 10^{-5}	2 6 10	2.4, 7.1, 11.9	0, 1 · 10^{-4}, 5.2 · 10^{-4}, 1.9 · 10^{-3}, 5.1 · 10^{-3}, 9.3 · 10^{-3}	0, 0.6, 3.1, 11.1, 30.8, 55.5	0, 100, 500, 1800, 5000, 9000
	CO_2	3.6 · 10^{-6} 1.2 · 10^{-5} 1.8 · 10^{-5}	1.3 3.95 6.58				
0.18 mm/ Teflon	Air	5.6 · 10^{-6} 1.7 · 10^{-5} 2.8 · 10^{-5}	2 6 10	2.4, 7.1, 11.9	0, 1 · 10^{-4}, 5.2 · 10^{-4}, 1.9 · 10^{-3}, 5.1 · 10^{-3}, 9.3 · 10^{-3}	0, 0.6, 3.1, 11.1, 30.8, 55.5	0, 100, 500, 1800, 5000, 9000
	CO_2	3.6 · 10^{-6} 1.2 · 10^{-5} 1.8 · 10^{-5}	1.3 3.95 6.58				
3.6 mm/ PEEK	Air	2.7 · 10^{-5} 8.1 · 10^{-5} 1.3 · 10^{-4}	9.7 29 48.4	11.5, 34.5 57.5	0, 1 · 10^{-4}, 5.2 · 10^{-4}, 1.9 · 10^{-3}, 5.1 · 10^{-3}, 9.3 · 10^{-3}	0, 0.6, 3.1, 11.1, 30.8, 55.5	0, 100, 500, 1800, 5000, 9000
	CO_2	1.8 · 10^{-5} 5.3 · 10^{-5} 8.8 · 10^{-5}	6.4 19.1 31.8				

3. Data processing

The recorded images were processed in DaVis 8.3 (LaVision) with a built-in shadow image processing tool combined with a Particle Tracking Velocimetry (PTV) algorithm. The detailed image processing steps can be found in (Kováts et al., 2020). Employing the distinct intensity gradients at the border of the focused and unfocused bubbles, only the bubbles were recognized, which were situated in the middle focused volume. From the processed data, equivalent sphere diameters (*ESD*), bubble velocities and their distributions have been obtained as shown e.g. in Fig. 2.

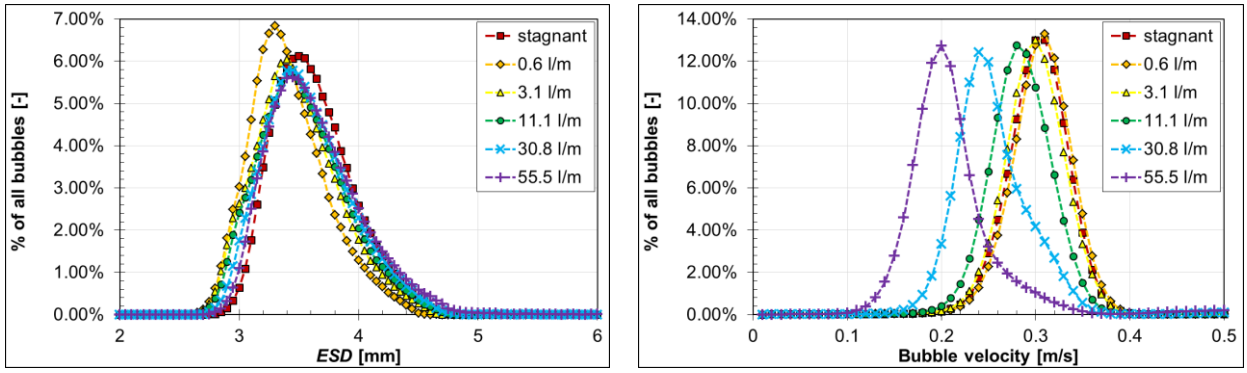

Fig. 2 Bubble *ESD* (left) and bubble velocity (right) distributions at different counter-current liquid flow conditions and 10 l/h air flow rate from 0.18 mm diameter capillaries.

This data has now been further evaluated to get more information, especially about bubble aspect ratio E with $E = h_b/l_b$, bubble inclination β and bubble velocity direction γ (see Fig. 3).

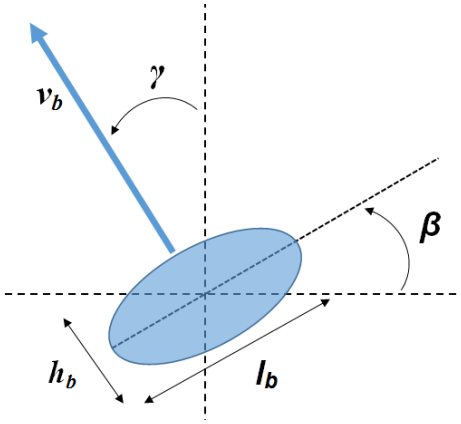

Fig. 3 Bubble parameters evaluated in this study.

For the statistical evaluations the bubble data has to be filtered. First, the bubbles were removed without determined bubble velocities. In the next step, the erroneously recognized bubbles (e.g. overlapping bubbles; as one big bubble recognized bubble clusters; etc.) were removed.

For the further data analysis the bubble data has to be reduced. Bubbles with the same equivalent sphere diameter do not have necessarily the same aspect ratios (see Fig. 4). Applying the postprocessing procedure described in details in (Kováts, 2021), mean aspect ratios were calculated for each equivalent sphere diameter (yellow circles on Fig. 4). This reduced data was used in the further calculations and comparisons.

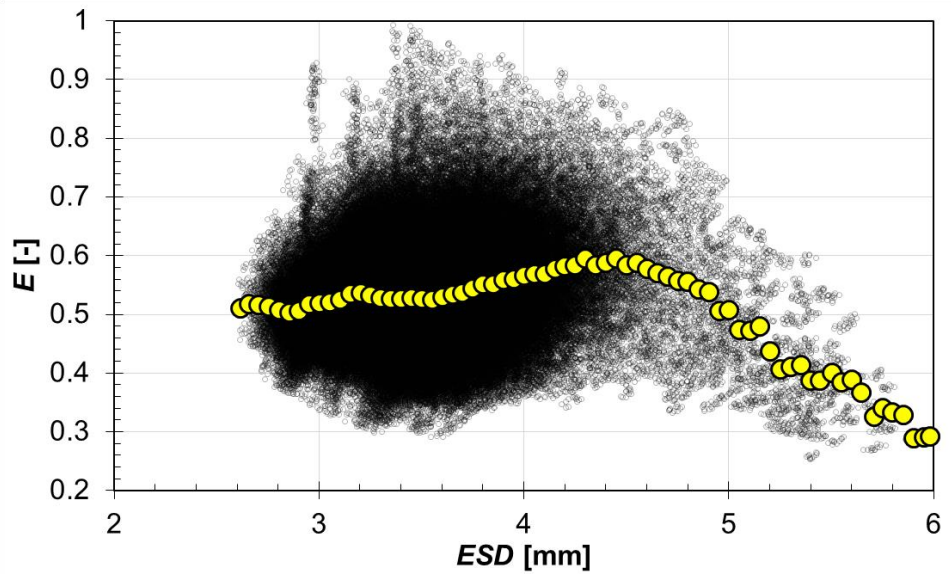

Fig. 4 Exemplary relationship between bubble aspect ratio *E* and the equivalent sphere diameter *ESD* at 6 l·h^{-1} air flow rate, 11.1 l·min^{-1} counter-current liquid flow and 0.18 mm capillary diameter. Yellow circles represent the mean aspect ratio.

4. Evaluation results

4.1. Equivalent sphere diameter (*ESD*)

The *ESD* results of the relatively badly soluble air and good soluble CO_2 bubbles show very different behaviour. An overview of the changes in the *ESD* of air bubbles is presented on Fig. 5. Here, and on all of the following figures in the legend first the capillary diameter is given, then the gas flow rate is referred with "g" and the liquid flow rate with "l". As expected, with larger capillary diameters larger bubbles were generated at the same gas and liquid volume flow rate (Fig. 5, a). The bubble diameters remain almost the same over the column height, just a slight growth can be recognized in the investigated length (1 m). This bubble growth is more visible on Fig. 5, b-d, due to the changed scale and is induced by the decrease of the hydrostatic pressure inside the column. Over the whole investigated height the diameter increases around 0.1 mm.

With increasing counter-current liquid flow the bubble size increases (Fig. 5, b). It is noticeable, that in the case of stagnant liquid similar bubble sizes have been found as at the highest, 55.5 $l \cdot min^{-1}$ counter-current liquid flow. This similarity was not observed with the 3.6 mm and 0.13 mm capillaries.

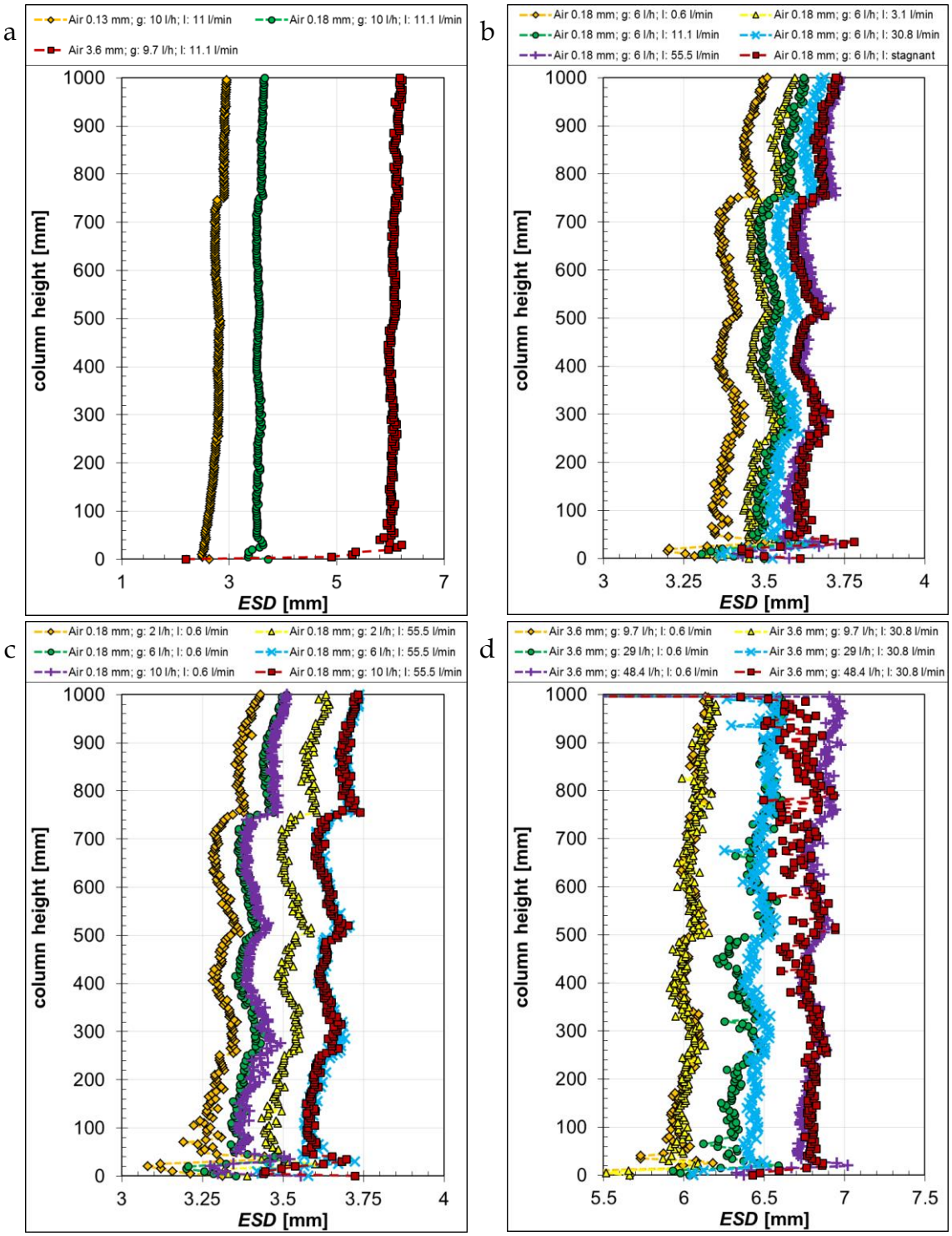

Fig. 5 An overview of the changes in the *ESD* of air bubbles, generated with different capillaries at different gas "g" and liquid "l" volume flow rates.

The influence of the gas volume flow rate is represented in Fig. 5, c and d. at two different counter-current liquid flows and for two different capillary sizes. The two counter-current liquid flows show similar results in the case of capillaries with 0.18 inner diameter. With increasing gas flow rate the bubble size increases, but the difference between 6 and 10 $l \cdot h^{-1}$ is negligible. The generated bubble size also increases at higher counter-current liquid flow (Fig. 5, c). Contrary to this, with the 3.6 mm capillaries, bubble sizes are not affected by the counter-current liquid flow, only the influence of the gas flow rate was observable (Fig. 5, d).

In contrast to the air bubbles, the CO_2 bubbles show a very different behaviour (Fig. 6). With increasing capillary size the generated bubble size increases, but due to the high solubility in water, the bubble size decreases over the column height continuously up to around 1mm (Fig. 6, a). The experiments have shown, that the bubbles reach a minimum size around 1 mm, then they do not shrink further (Fig. 6, a). Probably from these bubbles all CO_2 is dissolved into the liquid and the remaining bubble consist of the remaining and back diffused nitrogen. From this size also the automatic bubble recognition gets very difficult, because the shadows of these small bubbles are almost as bright as the background. Therefore, reliable bubble recognition was not possible under $ESD \approx 1$ mm and the representation on Fig. 6 is stopped.
As well as the air bubbles, the CO_2 bubbles are influenced by the counter-current flow (Fig. 6, b). But here, with increasing counter-current liquid flow the bubble size becomes smaller. The bubble shrinkage gradually increases with increasing counter-current liquid flow. The liquid-renewal on the bubble surfaces gets faster with increasing liquid flow rate, which enhances mass transfer from the bubbles into the liquid. Also the bubble residence time is increased, which also favourites its dissolution.
The influence of the gas flow rate on the generated bubble size is depicted at two different counter-current liquid flows on Fig. 6, c for the smallest capillary. With increasing gas flow rate the bubble size increases and gradually decreases to 1 mm over the height of the column. On this plot and also on Fig. 6, a it is observable, that bubble shrinkage runs parallelly for the same counter-current flow conditions. For this reason, it can be assumed that the mass transfer from the bubbles into the liquid is similar over the column height and does not depend on the initial bubble size, but the counter-current flow conditions. With the 3.6 mm capillaries the influence of the counter-current liquid flow and gas flow rate is similar to the air case (Fig. 6, d). With increasing gas flow rate the bubble size increases at the bottom of the column, but then bubble shrinkage decreases with the lower liquid flow rate. Therefore, at the column top, the bubble sizes differ strongly at the same gas flow rate between the different counter-current liquid flow rates.

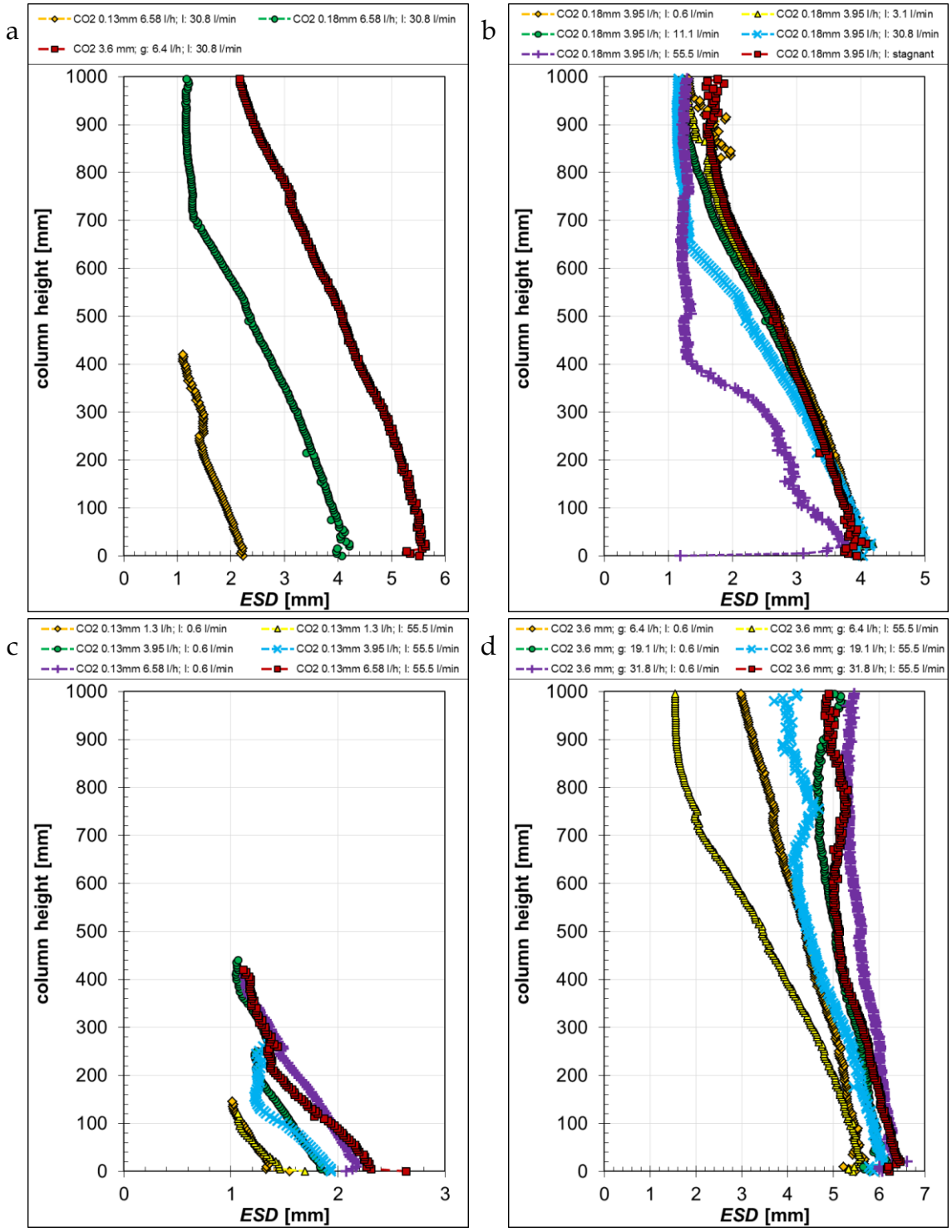

Fig. 6 An overview of the changes in the *ESD* of CO_2 bubbles, generated with different capillaries at different gas "g" and liquid "l" volume flow rates.

4.2. Bubble velocity

In the following, the measured bubble velocities will be analysed. Fig. 7 shows the air bubble velocities at different flow conditions.

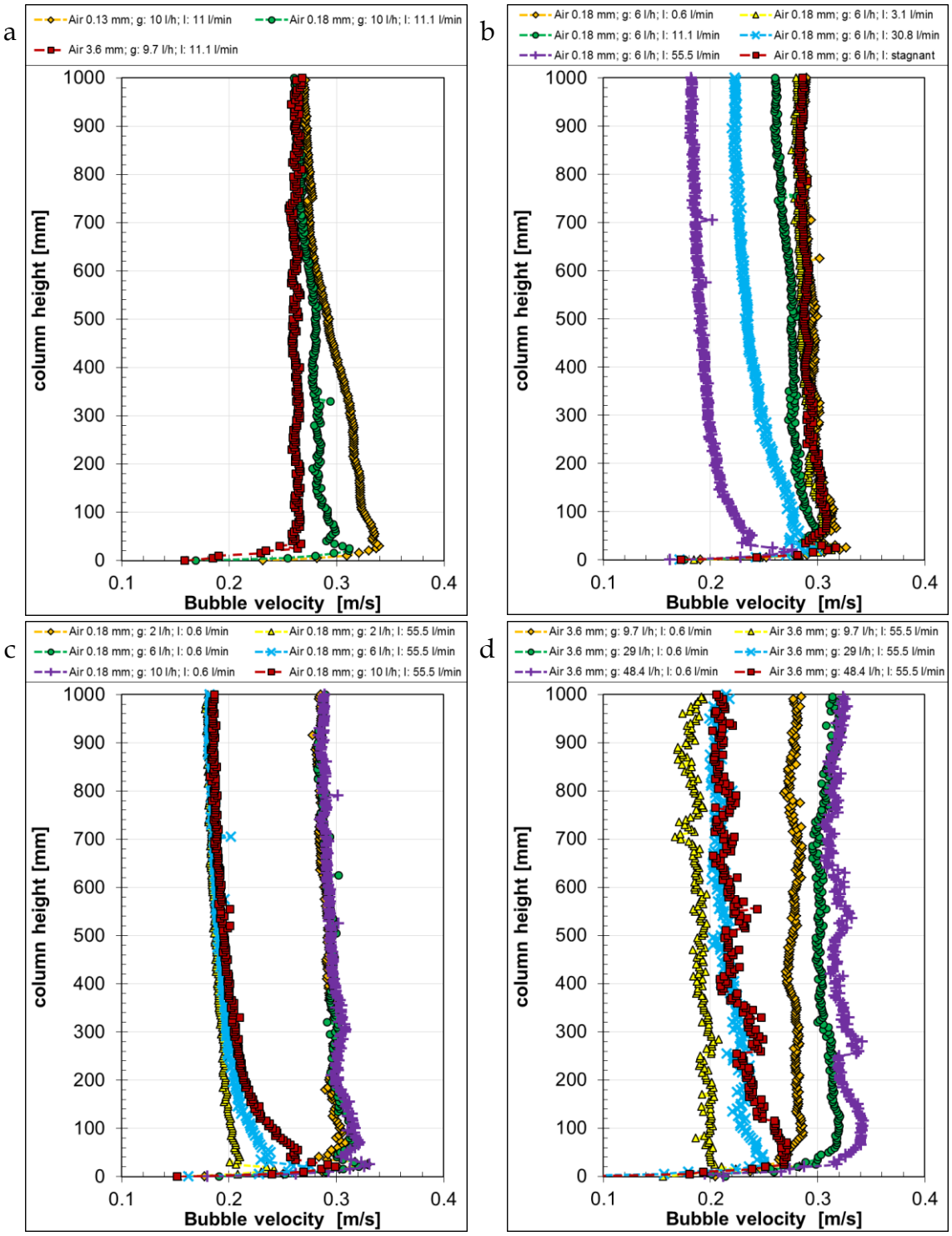

Fig. 7 An overview of the changes in the bubble velocity of air bubbles, generated with different capillaries at different gas "g" and liquid "l" volume flow rates.

Fig. 7, a represents the velocities of the bubbles generated with different capillaries. They differ just over the gas outlets, where the larger bubbles have lower velocities than the smaller ones. After about half the measurement section, all bubbles reach the same mean terminal velocity of about 0.27 $m \cdot s^{-1}$. With increasing counter-current liquid flow the bubble velocity decreases, but the velocity difference between the two smallest liquid flows and the stagnant condition is negligible (Fig. 7, b). Also the influence of the gas flow rate on the bubbles generated by smaller capillaries is negligible at low counter-current liquid flow (Fig. 7, c), while at the maximal counter-current liquid flow the starting velocity of the bubbles increases with increasing gas flow rate, until reaching similar terminal velocities at about half the column height. Due to the higher gas flow rate differences, the velocities of the bubbles generated by the 3.6 mm capillaries are more separated for the different flow conditions. With increasing gas flow rate the bubble velocity increases at the lowest, as well as at the highest counter-current liquid flow rate.

The velocities of the CO_2 bubbles show a larger variety (Fig. 8), due to the stronger size differences. With increasing capillary size, the bubbles starting velocities decrease. Then, according to the bubble shrinkage, the bubble velocities decrease differently over the column height (Fig. 8, a). With increasing counter-current liquid flow, the bubble velocity decreases over the complete column height (Fig. 8, b). According to the results of the PIV (Particle Image Velocimetry) measurements made with the same setup, the surrounding liquid flow has a larger influence on the bubble velocity change with increasing counter-current liquid flow than the velocity change due to the bubble size shrinkage, which effect is well noticeable on Fig. 8, b. With increasing gas flow rate the bubble starting velocity increases at the lowest, as well as at the highest counter-current liquid flow (Fig. 8, c and d). The velocity of smaller bubbles (< 3 mm) decreases stronger (Fig. 8, c and Fig. 8, d yellow triangles), while the velocity of the largest bubbles (>5 mm) remains almost the same over the investigated height (Fig. 8, d).

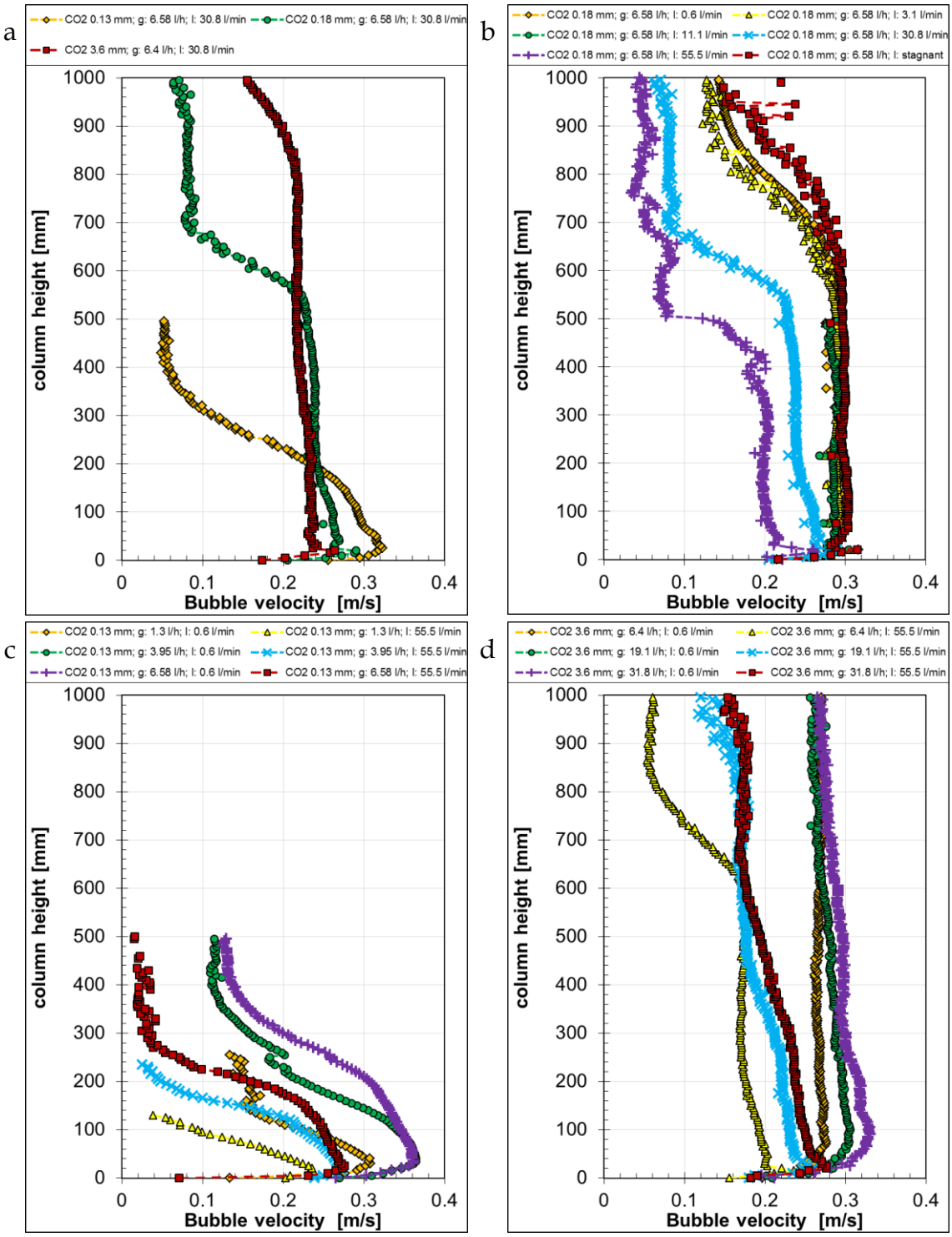

Fig. 8 An overview of the changes in the bubble velocity of CO_2 bubbles, generated with different capillaries at different gas "g" and liquid "l" volume flow rates.

4.1. Aspect ratio (*E*)

On the following two figures (Fig. 9 and Fig. 10) the bubble aspect ratio is plotted over the column height at different flow conditions for air and CO_2 respectively. In the case of air bubbles

the aspect ratio of the smallest bubbles generated by the 0.13 mm capillaries increases over the column height, while it remains almost the same for the two other capillary sizes (Fig. 9, a). After the bubbles leave the capillaries, the hydrostatic pressure gradually decreases and it has a visible influence on the aspect ratio of the small bubbles.

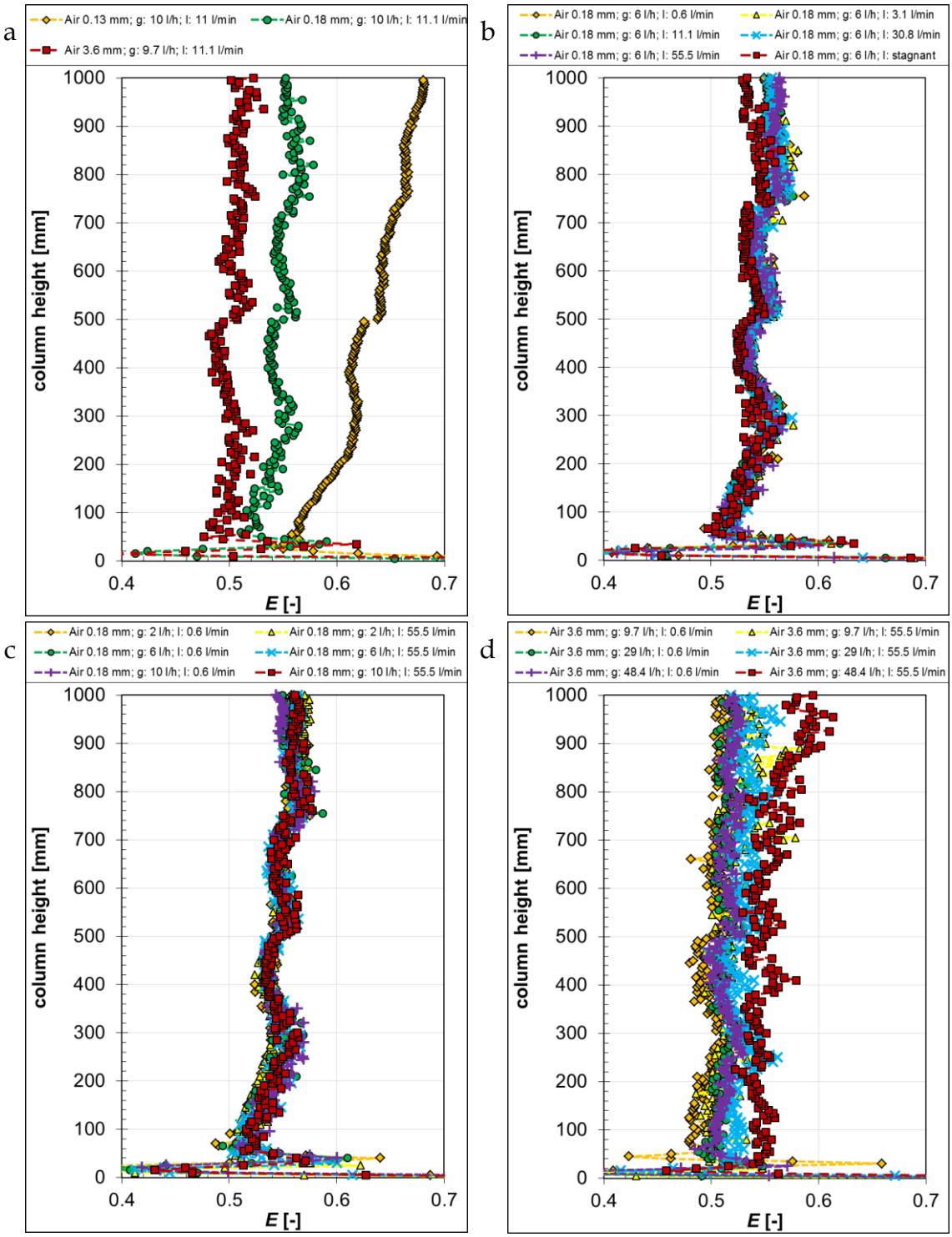

Fig. 9 An overview of the changes in the aspect ratio *E* of air bubbles, generated with different capillaries at different gas "g" and liquid "l" volume flow rates.

For larger bubbles, the decreasing hydrostatic pressure has no visible effect on the bubble deformation and form. After the bubbles leave the capillaries, the aspect ratio is always the lowest, around 0.5, due to surface fluctuations.

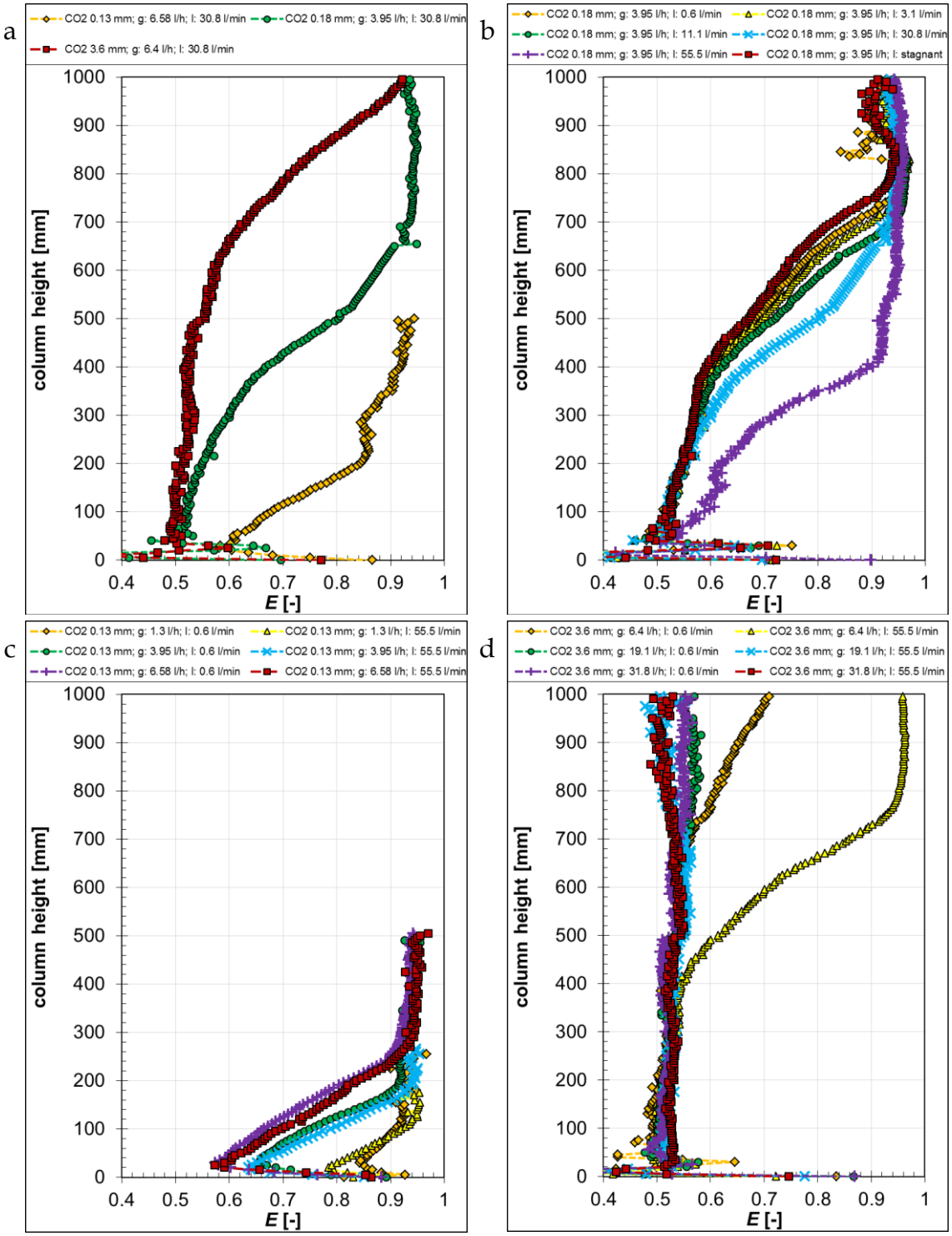

Fig. 10 An overview of the changes in the aspect ratio *E* of CO_2 bubbles, generated with different capillaries at different gas and liquid volume flow rates.

After around 300 mm, this surface wobbling is damped. It is worth to point out, that neither the counter-current liquid flow rate (Fig. 9, b), nor the gas flow rate (Fig. 9, c) influence significantly the aspect ratio of the bubbles. Only for the largest bubbles at the highest liquid counter flow rate a difference is observable (Fig. 9, d).

In the case of the CO_2 bubbles the aspect ratio change is dominated by the bubble shrinkage (Fig. 10). With decreasing capillary size the aspect ratio increases, as well as due to the bubble shrinkage over the column height (Fig. 10, a). Since the counter-current liquid flow influences the bubble shrinkage, the aspect ratio increases also, but no differences can be found for the aspect ratio of the bubbles which just leave the capillaries (Fig. 10, b). However, with increasing gas flow rate the aspect ratio of the small CO_2 bubbles decreases at the outlet (Fig. 10, c), while it remains similar for the bigger bubbles (Fig. 10, d), where it only increases in the higher sections of the column for the small gas flow rate.

4.3. Bubble inclination (β) and velocity direction (γ)

Some examples of results for distributions of the bubble inclination and velocity direction for air and CO_2 bubbles in stagnant liquid and at different counter-current liquid flow conditions are shown in the following in function of the column height (Fig. 11 and Fig. 12 respectively). In these figures, some regions do not contain any data (dark blue horizontal lines). Practically these regions are the overlapping regions of the camera views and these regions were removed from the data processing to avoid false statistical results. The colourbars correspond to the number of events. On the left side of the distributions, the RMS over the column width is represented.

In the exemplary air bubble cases at same gas flow rate but different counter-current liquid flow (left column in Fig. 11), the bubble inclination β range and RMS-value are nearly the same. Only the number of events changes with increasing counter flow rate, due to a longer residence time of the bubbles. In contrast, the range of velocity direction γ and its RMS increase with increasing counter-current liquid flow. This change indicates the more wobbling motion of the bubbles with higher counter-current liquid flow.

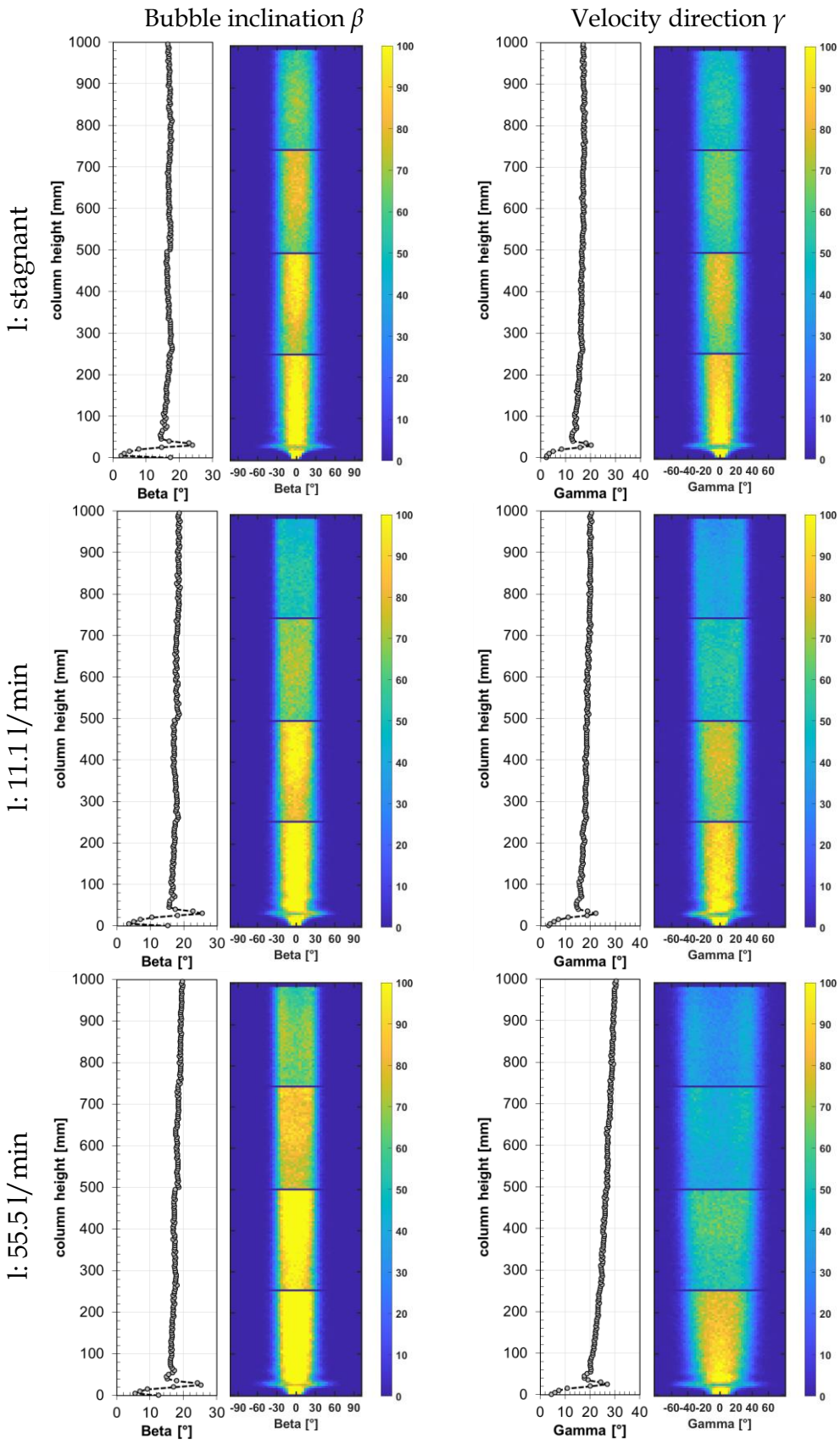

Fig. 11 Number densities and RMS values in function of column height for bubble inclination β and velocity direction γ for air bubbles from 0.18 mm capillaries at 6 l/h gas flow rate and different liquid flow rates.

In the exemplary CO_2 bubble cases the bubble inclinations β show similar distributions up to a certain height, where the bubbles reach a diameter around 1-1.5 mm (Fig. 12, left column). Since at this size they are spherical, a reliable determination of the bubble inclination is no more possible (red rectangles in the images). This position is related to a RMS value of $\beta \geq 45°$. Contrary to the bubble inclination, the determination of the velocity direction is still possible for the small spherical bubbles. With decreasing bubble size (increasing column height) the bubble inclination decreases also and tends to zero in the top section of the bubble column in the stagnant liquid and at 11.1 10 $l \cdot min^{-1}$ counter-current liquid flow rate. At 11.1 $l \cdot min^{-1}$ counter-current liquid flow rate the bubble size decreases faster than in the case of a stagnant liquid, therefore the bubble motion become straight earlier. At 55.5 $l \cdot min^{-1}$ counter-current liquid flow rate, the bubbles were almost stopped by the liquid flow at around 500 mm (please refer to Fig. 8, b) and forced to move sidewards, therefore the velocity direction angle, as well as its RMS, becomes larger in this region.

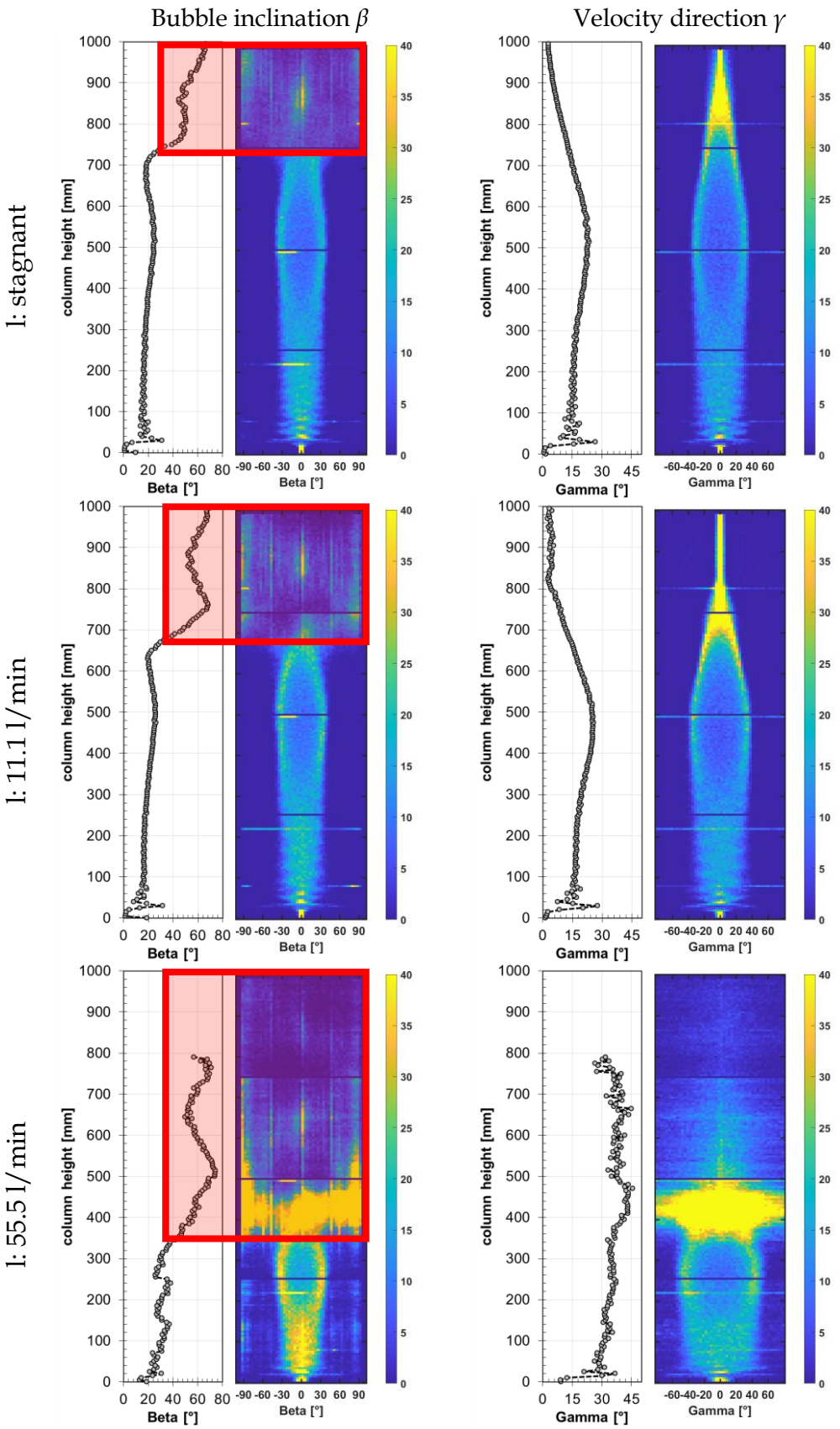

Fig. 12 Number densities and RMS values in function of column height for bubble inclination β and velocity direction γ for CO_2 bubbles from 0.18 mm capillaries at 1.3 l/h gas flow rate and different liquid flow rates.

4.3. Mean bubble diameters and aspect ratios for all cases

Mean aspect ratios and bubble diameters are finally determined from all measurement results as mentioned in section 3, Fig. 4, in order to compare these results to empirical correlations for bubble aspect ratio (Fig. 13 and Fig. 14).
It is clearly visible, that with different capillary sizes, different bubble aspect ratios are reached, however the results of air and CO_2 bubbles for each capillary are similar (see symbols in Fig. 13 and Fig. 14). These mean aspect ratios are compared to some empirical correlations from the literature (see lines in Fig. 13 and Fig. 14).

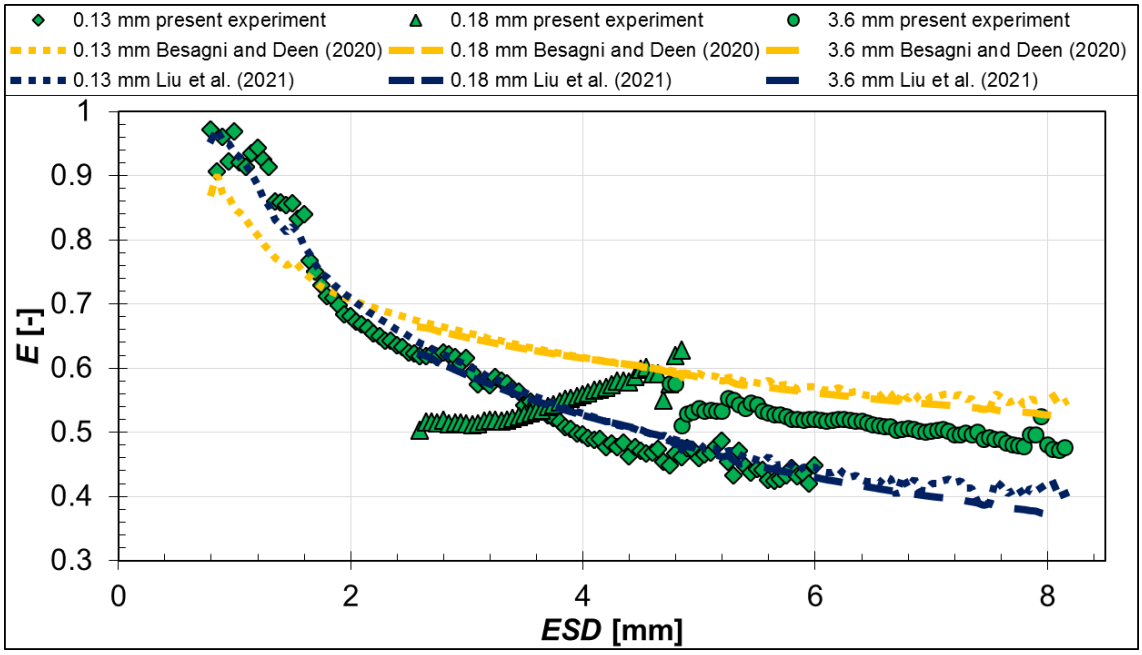

Fig. 13 Relationship between bubble aspect ratio *E* and equivalent sphere diameter *ESD* for air bubbles.

In the case of air bubbles (Fig. 13), the correlation of (Besagni & Deen, 2020) underestimates the aspect ratio for bubble diameters up to about 2mm, while it overestimates the bubble aspect ratios for nearly all cases over 2 mm. The correlation of (Liu et al., 2021) performs better, however it can predict just the bubble aspect ratios, generated with the 0.13 mm capillaries. In the other two cases, the aspect ratios are underestimated.

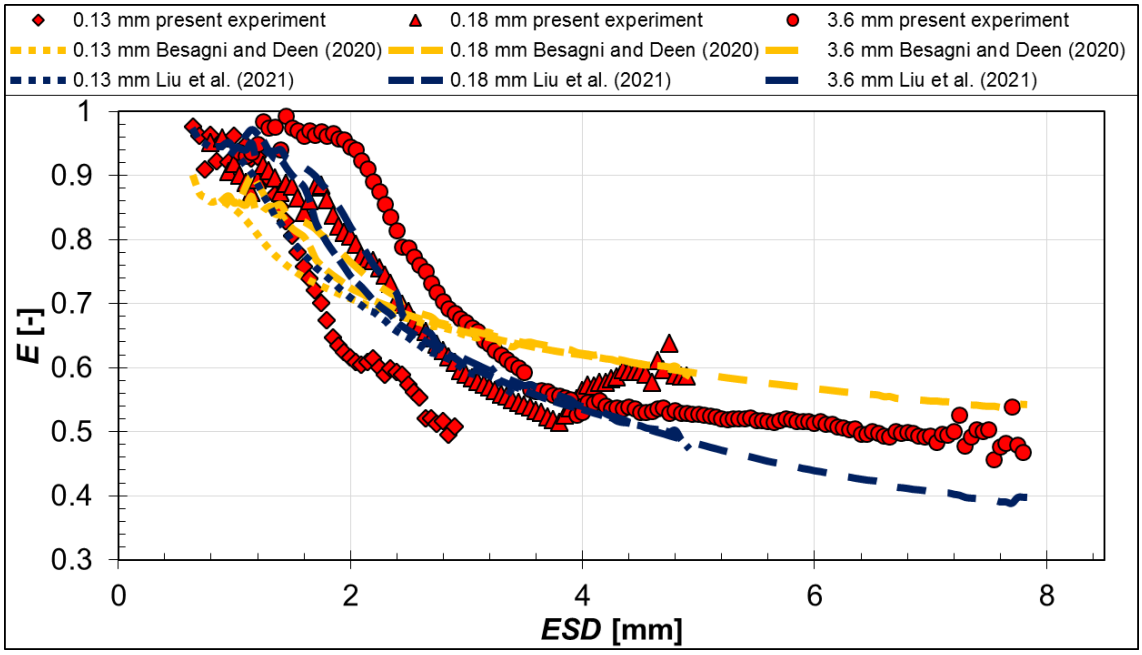

Fig. 14 Relationship between bubble aspect ratio *E* and equivalent sphere diameter *ESD* for CO_2 bubbles.

In the case of CO_2 bubbles (Fig. 14) both of the correlations under- and overestimate the experimental results, none of them can predict the aspect ratio in the whole bubble size range. However, they capture well the decreasing trend of the aspect ratio with increasing bubble diameter. This shows the necessity of more sophisticated correlations, taking into account the gas and liquid properties, as well as the bubble generation conditions.

5. Conclusions

In this study shadow imaging experiments of bubbles rising in pure water with and without counter-current liquid flow have been acquired and evaluated to deliver statistical data of bubble diameter, bubble aspect ratio, bubble orientation, motion direction and bubble velocity. In the measurements two types of gases –relatively badly soluble air and good soluble CO_2 – are applied. Moreover three different capillary diameters were used to generate bubbles in a wide diameter range from around 1.5 to 6.5 mm.

The strong influence of the counter-current liquid flow on the bubble rising behaviour is obvious from these results. It has been found that the counter-current liquid flow has a large effect on the bubble velocity and motion direction but also noticeably influences the generated bubble diameter. Interestingly, the effect of the counter-current liquid flow on the aspect ratio of air bubbles is negligible. However, in the experiments with CO_2 bubbles a significant bubble aspect ratio change has been observed, due to the bubble shrinkage. It has also been found that the increased counter-current liquid flow is beneficial for the mass transfer. The statistics have been

obtained in function of the column height and will serve for the determination of correlations needed in numerical calculations and modelling.

Acknowledgements

Authors would like to thank their student Steffen Erichson for his help in doing the original experiments and Anselm Dreher for programming the evaluation routines. The financial support of the German Research foundation (DFG) under grant No. ZA 527/3-1 is gratefully acknowledged.

References

Besagni, G., & Deen, N. G. (2020). Aspect ratio of bubbles in different liquid media: A novel correlation. *Chemical Engineering Science, 215*, 115383. doi:10.1016/j.ces.2019.115383

Kováts, P. (2021). *Detailed experimental study of mass transfer and liquid flow in a bubble column with optical measurement techniques.* (PhD), Otto-von-Guericke-Universität Magdeburg, Magdeburg.

Kováts, P., Thévenin, D., & Zähringer, K. (2020). Influence of viscosity and surface tension on bubble dynamics and mass transfer in a model bubble column. *International Journal of Multiphase Flow, 123*, 103174. doi:10.1016/j.ijmultiphaseflow.2019.103174

Liu, L., Zhang, H., Yan, H., Ziegenhein, T., Hessenkemper, H., Zhou, P., & Lucas, D. (2021). Experimental studies on bubble aspect ratio and corresponding correlations under bubble swarm condition. *Chemical Engineering Science, 236*, 116551. doi:10.1016/j.ces.2021.116551

Mühlbauer, A., Hlawitschka, M. W., & Bart, H. J. (2019). Models for the Numerical Simulation of Bubble Columns: A Review. *Chemie Ingenieur Technik, 91*(12), 1747-1765. doi:10.1002/cite.201900109

Rzehak, R., Krauss, M., Kovats, P., & Zahringer, K. (2017). Fluid dynamics in a bubble column: New experiments and simulations. *International Journal of Multiphase Flow, 89*, 299-312. doi:10.1016/j.ijmultiphaseflow.2016.09.024

Sommerfeld, M., Muniz, M., & Reichardt, T. (2018). On the Importance of Modelling Bubble Dynamics for Point-mass Numerical Calculations of Bubble Columns. *Journal of Chemical Engineering of Japan, 51*(4), 301-317. doi:10.1252/jcej.17we277